NASA CR-66675

THE DEVELOPMENT OF AN ALL-PNEUMATIC WIDE ANGLE FREE GYROSCOPE

By W. H. Henley

Prepared under Contract No. NAS1-7570 by
CONDUCTRON CORPORATION
Western Development Center
Northridge, California

for

NATIONAL AERONAUTICS AND SPACE ADMINISTRATION

July 1968

NASA CR-66675

THE DEVELOPMENT OF AN ALL-PNEUMATIC WIDE ANGLE FREE GYROSCOPE

By W. H. Henley

Prepared under Contract No. NAS1-7570 by
CONDUCTRON CORPORATION
Western Development Center
Northridge, California

for

NATIONAL AERONAUTICS AND SPACE ADMINISTRATION

July 1968

TABLE OF CONTENTS

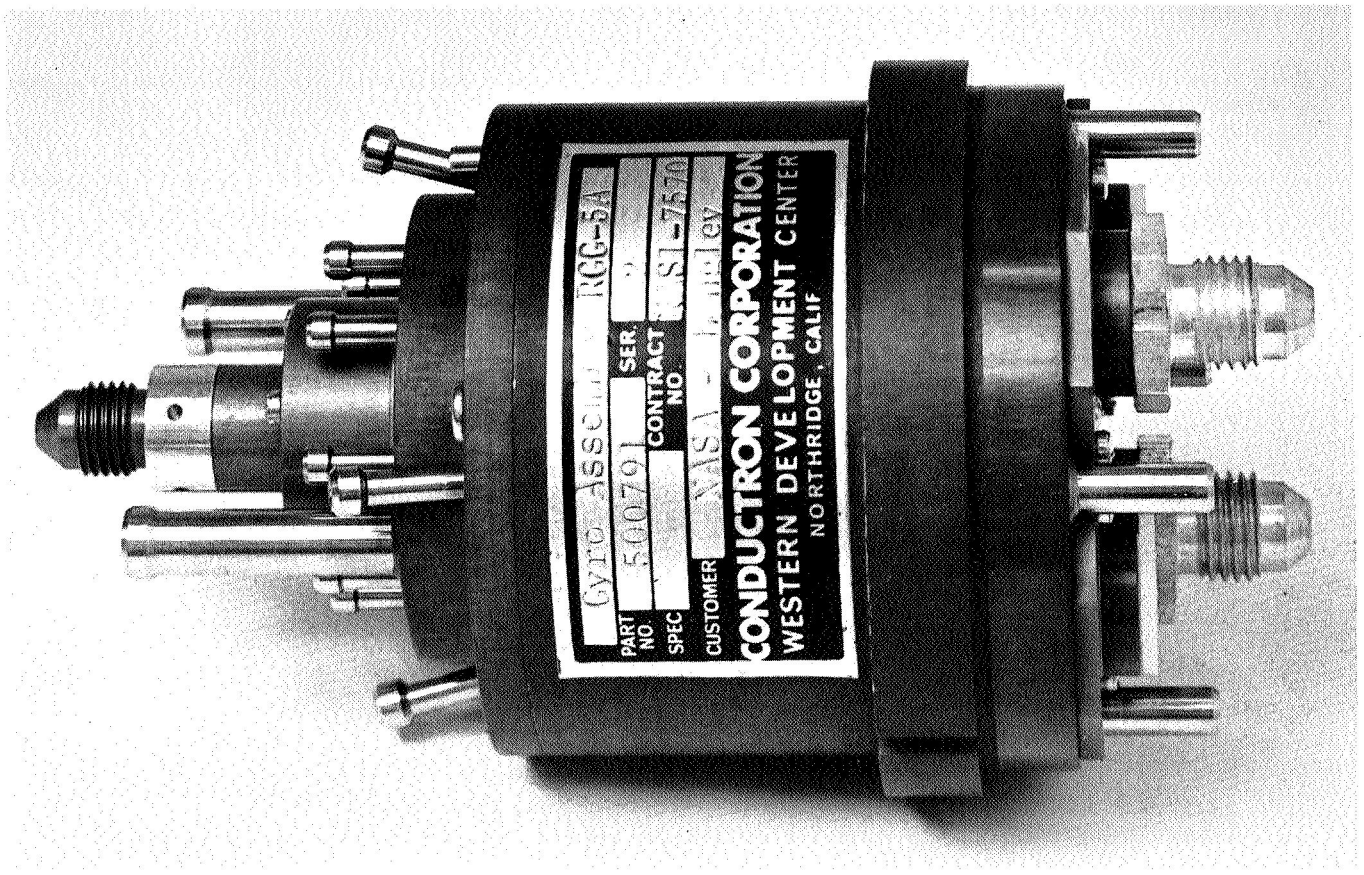

FIGURE 1 RGG-5A GYRO

THE DEVELOPMENT OF AN ALL-PNEUMATIC WIDE ANGLE FREE GYROSCOPE

By W. H. Henley
Conductron Corporation

SUMMARY

In this program, two all-pneumatic free gyroscopes were designed, constructed, and delivered to the National Aeronautics and Space Administration. These gyroscopes incorporated wide angle gas bearing supports, reaction-jet rotor spin motors, wide angle two-axis fluidic pickoffs, and fluidic main and bias torquers.

The two delivered units were subjected to a thorough test program to evaluate their performance relative to the following work statement goals:

1. 0.5 to 1.0 degree/hour drift.
2. Plus or minus 15 degree operating freedom.
3. Erection alignment capability of 2 to 3 arc-minutes.
4. Spin-up and alignment time of 5 to 10 minutes.
5. Maximum precession capability of torquer, 30 degrees/minute.

INTRODUCTION

The purpose of the program covered by this report was to design, construct, and evaluate an all-pneumatic, free gyroscope. The performance goals specified were derived from the general requirements for the secondary strap-down attitude reference for space probe vehicles of the Lunar Orbiter class. The basic design concepts for the new component elements of such a device were investigated under a previous National Aeronautics and Space Administration contract, NAS1-6533, and shown to be feasible. The present program expanded on those concepts and integrated all of the component elements into a complete gyro package, Figure 1. Two units of this design were built, tested, and delivered to NASA.

Fluidic guidance and control systems potentially offer a number of advantages, including low cost, ruggedness, sterilizability, and the ability to survive and operate in severe thermal and radiation environments. For this reason, a number of fluidic inertial reference devices have been designed and built by various organizations. The present gyro, however, is the first fluidic unit to demonstrate 1 degree/hour total drift rate performance over a narrow angular range, and to provide all gyro functions, including torquing, over a $\pm$ 15 degree angular range.

The writer wishes to acknowledge the vital part played in the program by his colleagues at Conductron Corporation, particularly Messrs. Philip A. Christopher, William J. Gross, and Burton D. Swirsky.

GYRO DESIGN

The RGG-5A Gyro is a two-degree-of-freedom device in which all of the conventional functions of rotor support, spin-up, position pickoff, and torquing are performed pneumatically. As shown schematically in Figure 2, the rotor is supported on a central spherical hydrostatic air bearing and spun-up, lawn sprinkler-like, by a pair of reaction jets. The rotor is precessed on demand by jets of air impinging on its external surface. The pneumatic wide angle pickoff capability is provided by four separate thin slots in the surface of a spherical cavity. A protuberance on the spin axis of the rotor fits closely in this cavity and blocks the slots differentially, depending on the rotor angular position. Four small holes on axes rotated 45 degrees from the axes of the slots operate in the same way to provide higher gain output signals around the rotor null position. Two windows in the case provide an independent visual indication of rotor attitude and, by means of markings on the rotor, allow rotor speed determination by a strobo-tach. These components are packaged in a cylindrical case 2-1/2 inches in diameter by 3-5/8 inches long, as shown in Figure 3. The design and functional characteristics of each of these components is discussed at greater length in the following sections. The design parameters of the assembly are summarized in Table 1 below.

TABLE 1

Gyro Parameters

Rotor Polar Moment of Inertia -	2.13×10^{-4} in-lb-sec^2
Rotor Operating Speed -	20,000 rpm
Rotor Angular Momentum -	4.46×10^{-1} in-lb-sec
Wide Angle Pickoff Gain -	4.2×10^{-2} psid/deg
Torquer Scale Factor -	2.2×10^{4} deg/minute/psig/rpm^{-1}
Calculated Gas Comsumption (torquers off) -	1.0 scfm
Air Bearing Supply Pressure -	40 psig
Spin Pressure -	26 psig

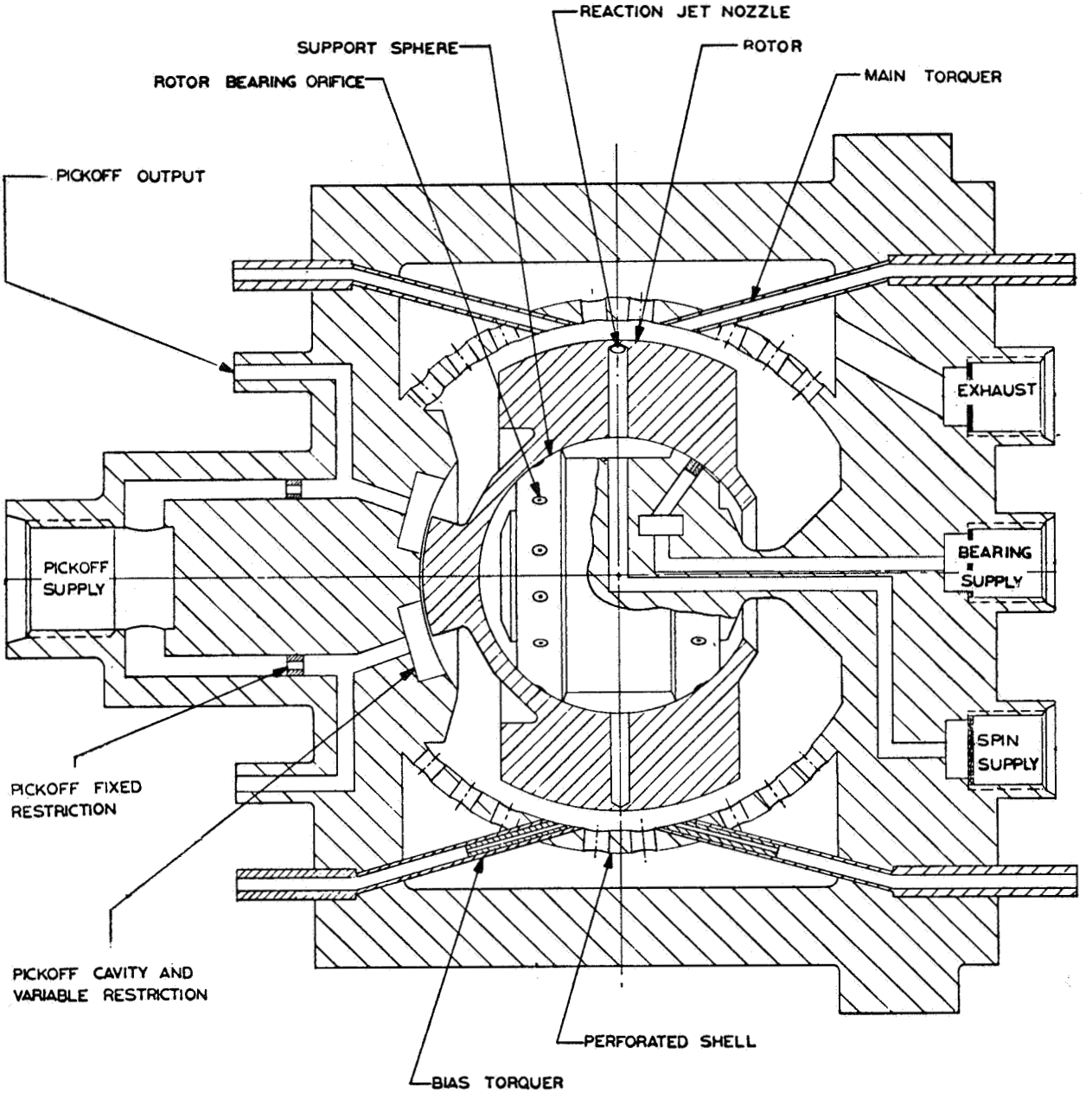

SCHEMATIC RGG-5A GYRO

FIGURE 2

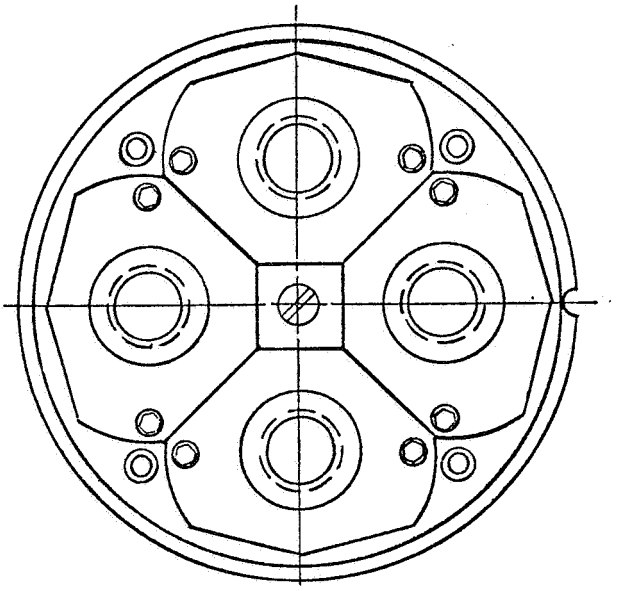

END VIEW

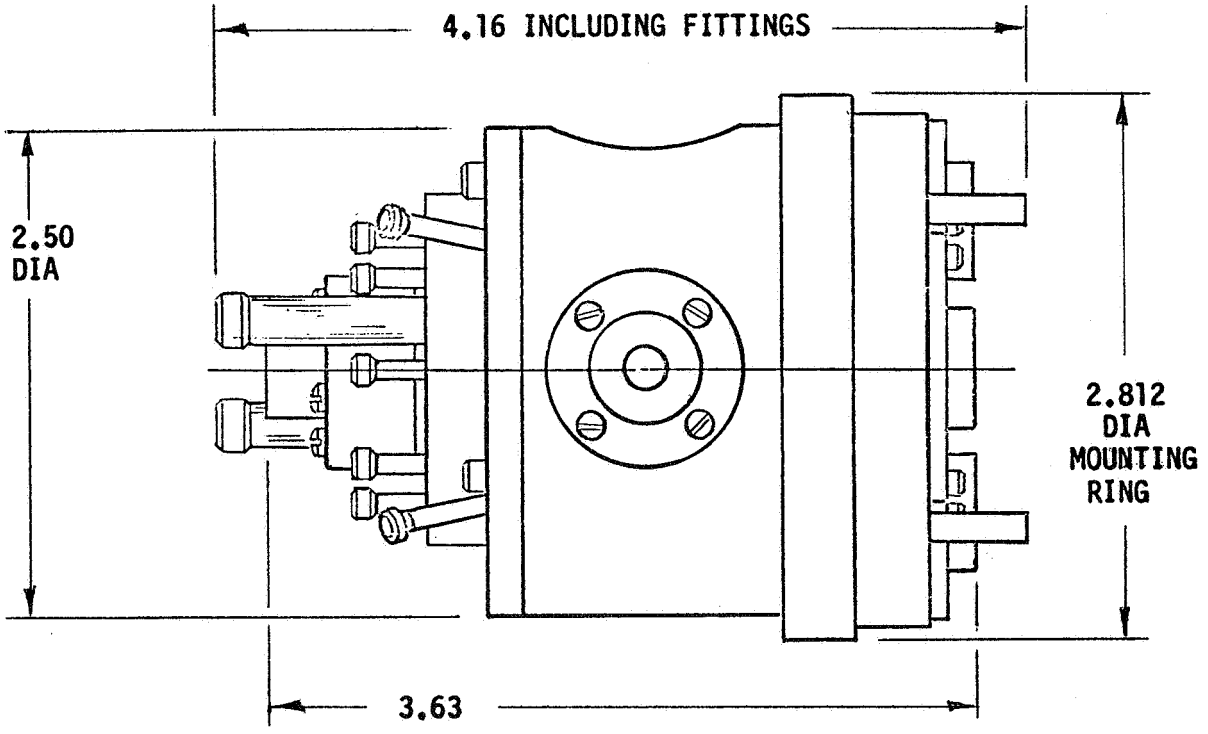

SIDE VIEW

OUTLINE DRAWING RGG-5A GYRO

FIGURE 3

Wide Angle Air Bearing

One of the objectives of the design of the RGG-5A Gyro is a ± 15 degree angular excursion of the rotor. The design technique employed is to utilize an isotorsional bearing geometry, as described in detail in Reference 1, consisting of spherical bearing bands on the stator, bounded by latitude circles symmetrically located about the stator equator and enveloped by a spherical cavity in the rotor which overhangs these bands by more than 15 degrees, so that the rotor experiences no inherent self-aligning torque regardless of its orientation. Each spherical bearing band is supplied with pressurized air via twelve fixed restrictors equally spaced along a circle parallel to the band boundaries, whose latitude angle is selected to provide an isoelastic suspension. In order to minimize turbine torques due to asymmetrical flow patterns within the air bearing, a novel construction was adopted for the bearing restrictors. As shown in the sketch below, the primary flow restriction is a commercial .0031 inch I.D. synthetic ruby ring jewel. The flow then passes through a fine filter paper with the object of breaking up the high velocity jet from the primary restrictor and diffusing the flow so that the pressure at the bearing surface is substantially equal everywhere within the recess feeding the bearing.

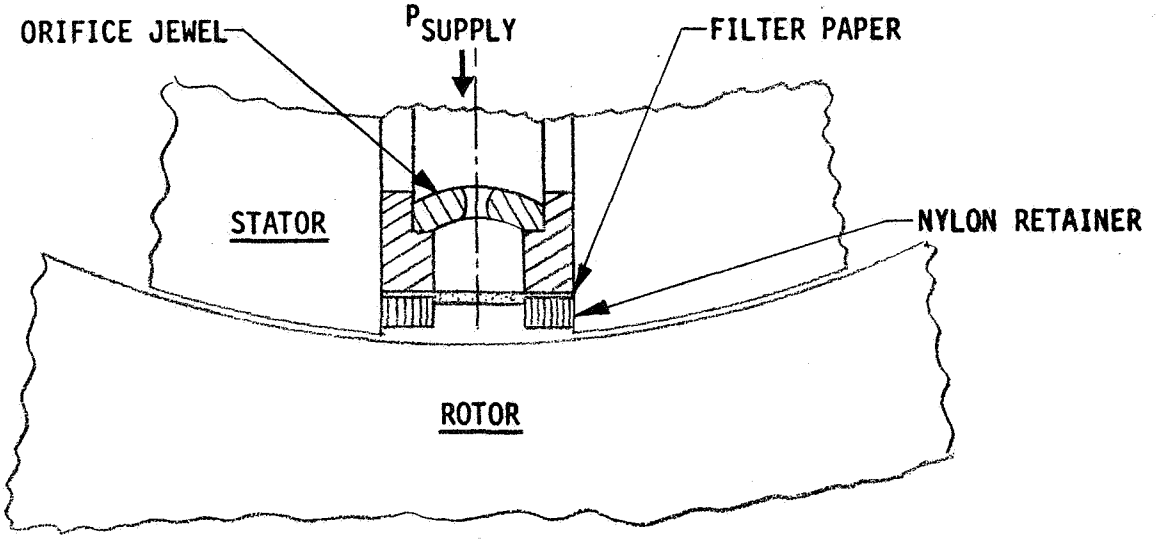

AIR BEARING RESTRICTOR DESIGN

The design radial clearance between the rotor and stator is .0003 inch, providing a relatively stiff bearing, but necessitating close control on possible particle contaminants. A clear advantage of the built-up restrictor configuration described above is the protection afforded by the filter element in each restrictor, which prevents any particles from exiting the bearing supply system directly into the bearing gap.

Torquers

The RGG-5A Gyro, as shown schematically in Figure 2, has two sizes of torquers; one set for precessing the rotor at a commanded rate up to 30 degrees/minute, and the other set to provide constant bias torques to the rotor to overcome systematic drift-producing torques present in the unit. The sizing and detail design of the torquers is based on the experimental results obtained in the feasibility program reported in Reference 1. Essentially, torquing of the rotor is achieved by directing jets of air approximately tangentially to the surface of the rotor perpendicular to the rotor equator. Control of the torque exerted on the rotor is exercised by: a) size of the torquer nozzle; b) applied pressure; and c) selection of the torquer, or combination of torquers, to be activated.

Torquer sizing calculations.--The design criteria for the torquers was selected as achievement of a rotor precession rate of 30 degrees/minute, or 8.73×10^{-3} radians/second, at an applied pressure of 30 psig. The angular momentum, H, of the rotor at the design speed of 20,000 rpm was calculated to be equal to 0.446 in-lb second. The torque, T, required of the torquer was found by substituting the given values for H and $\dot{\theta}$, the rotor precession rate, into the scalar gyroscopic relation:

$$T = H\dot{\theta} \tag{1}$$

$$T_{max} = (4.46 \times 10^{-1})(8.73 \times 10^{-3}) = 3.89 \times 10^{-3} \text{ lb-in.} \tag{2}$$

From Reference 1, the weight flow, $\dot{w}_j$, required, for a 20 degree inclination of the jet, can be found from the equation:

$$\dot{w}_j = \frac{T g}{.42\ Vr \cos 20^o} \tag{3}$$

where g is the acceleration due to gravity, 386 in/sec^2; V is the jet velocity, 1.32×10^4 in/sec for sonic flow; r is the jet radius, .75 inches. Substituting numerical values in Equation (3), the required torquer jet flow is found:

$$\dot{w}_j = \frac{(3.89 \times 10^{-3})(386)}{(0.42)(1.32 \times 10^4)(0.75)(.9397)} = 3.84 \times 10^{-4} \text{ lb/sec} \tag{4}$$

The torquer sizing can now be established. The standard equation for sonic flow can be written:

$$\dot{w}_j = \frac{.532\ A_1 C_D\ P_t}{\sqrt{S_t}} \tag{5}$$

where A_1 is the torquer jet area, inches^2; C_D is the discharge coefficient; P_t is the applied pressure, psia; and S_t is the temperature of the air, degrees Rankine. Rearranging:

$$A_1 = \frac{\dot{w}_j \sqrt{S_t}}{.532\ C_D\ P_t} \tag{6}$$

$$A_1 = \frac{(3.84 \times 10^{-4}) \sqrt{520}}{(.532)\ (.81)\ (45)} = 4.52 \times 10^{-4}\ \text{in}^2 \tag{7}$$

The torquer inside diameter, D_1, is then:

$$D_1 = .024 \text{ inches}$$

The bias torquers can be sized by the same procedure. However, the bias torquer sizing also can be found by direct ratio to that of the main torquers. Assuming a maximum value of bias torque equal to that required to precess the rotor 30 degrees/hour at 30 psig, the flow area required is $1/60$ of that required by the main torquers, so the area, A_2, and diameter, D_2, are:

$$A_2 = 4.52 \times 10^{-4}/_{60} = 7.53 \times 10^{-6}\ \text{in}^2$$

$$D_2 = .003 \text{ inches}$$

Because of tubing size limitations, it was necessary to select an actual diameter, D_2 = .004 inches, providing a design bias torquer capability, T_B, at 30 psig of:

$$T_B = 30 \times 60 \times \left(\frac{.004}{.024}\right)^2 = 50 \text{ degrees/hour} \tag{8}$$

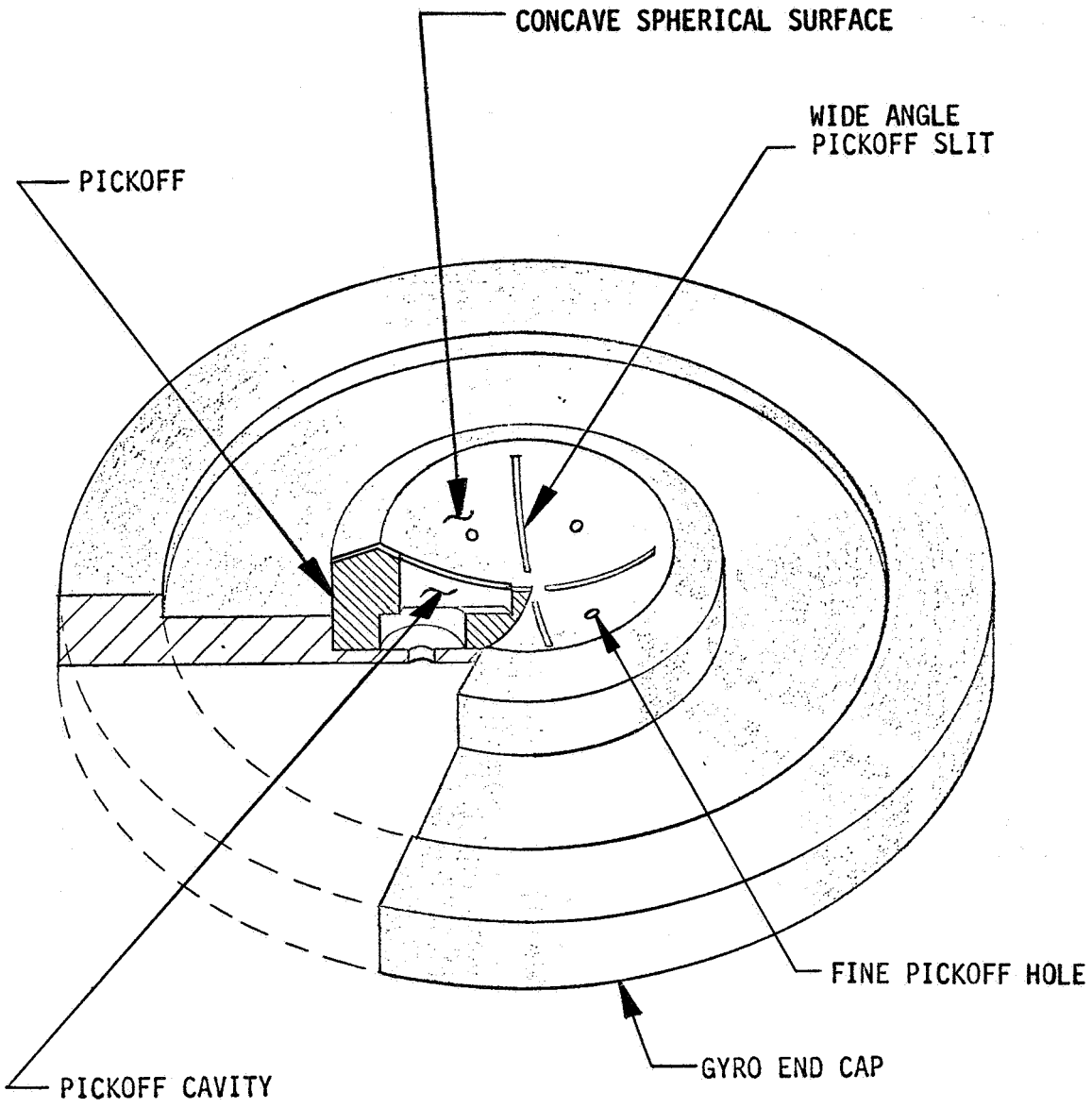

PICKOFF CONSTRUCTION

FIGURE 4

Pickoffs

Two sets of pickoffs are provided on the RGG-5A Gyro; a set of wide angle pickoffs with a linear range of ± 15 degrees, and a set of fine pickoffs with a high gain around null. These pickoffs are essentially pneumatic pressure dividers, each consisting of a fixed first resistance in series with a variable second resistance whose value is established by rotor position. A regulated input pressure is applied upstream of the fixed resistance, and the pickoff output pressure is taken off between the two resistances so that its value increases as the downstream variable resistance increases.

The variable resistance consists of an opening in a concave spherical shell, closely concentric to a mushroom-shaped protrusion along the spin axis of the rotor, Figure 2, and aligned with the rotor so that the flow area of the variable resistance is defined by that part of the opening not covered by the rotor. As the rotor moves to close off the opening, its resistance increases, due to increased flow blockage; and the output pressure rises proportionately. Two such pickoffs are employed for each sensitive axis, one on each side of the rotor, so that one output pressure rises while the other falls in response to rotor movement. The differential pressure between these two provides the rotor position indication.

The variable resistance elements employed in the wide angle pickoffs are long, thin slits, as shown schematically in Figure 4. Four of these pickoffs at 90 degrees to each other provide complete two-axis information on the rotor angular position over the range of ± 15 degrees. The fine pickoff variable resistance elements are small diameter holes lying on axes 45 degrees displaced from the wide angle pickoffs, and located so that half of the hole is covered by the rotor at its null position. Because of their smaller size and their intended use during the closed-loop erection mode only, the supply pressure to the fine pickoffs can be higher without creating unacceptable coercive torques on the rotor. The small rotor angular excursion required to traverse the full range of these variable resistance elements from open to closed, combined with the higher supply pressure allowable, provide the potential of resolving rotor angular position at null with extreme sensitivity. This degree of resolution is not required to meet the present goals, but was included to facilitate implementation of a separate closed-loop rotor erection system.

Windows

A unique feature of the design of the RGG-5A Gyroscope is the provision of two plastic windows in the case, which allow direct visual observation of the rotor during operation. These two windows are set at 90 degrees to each other, so as to coincide with the wide angle pickoff axes and are located directly over the center of rotation of the rotor.

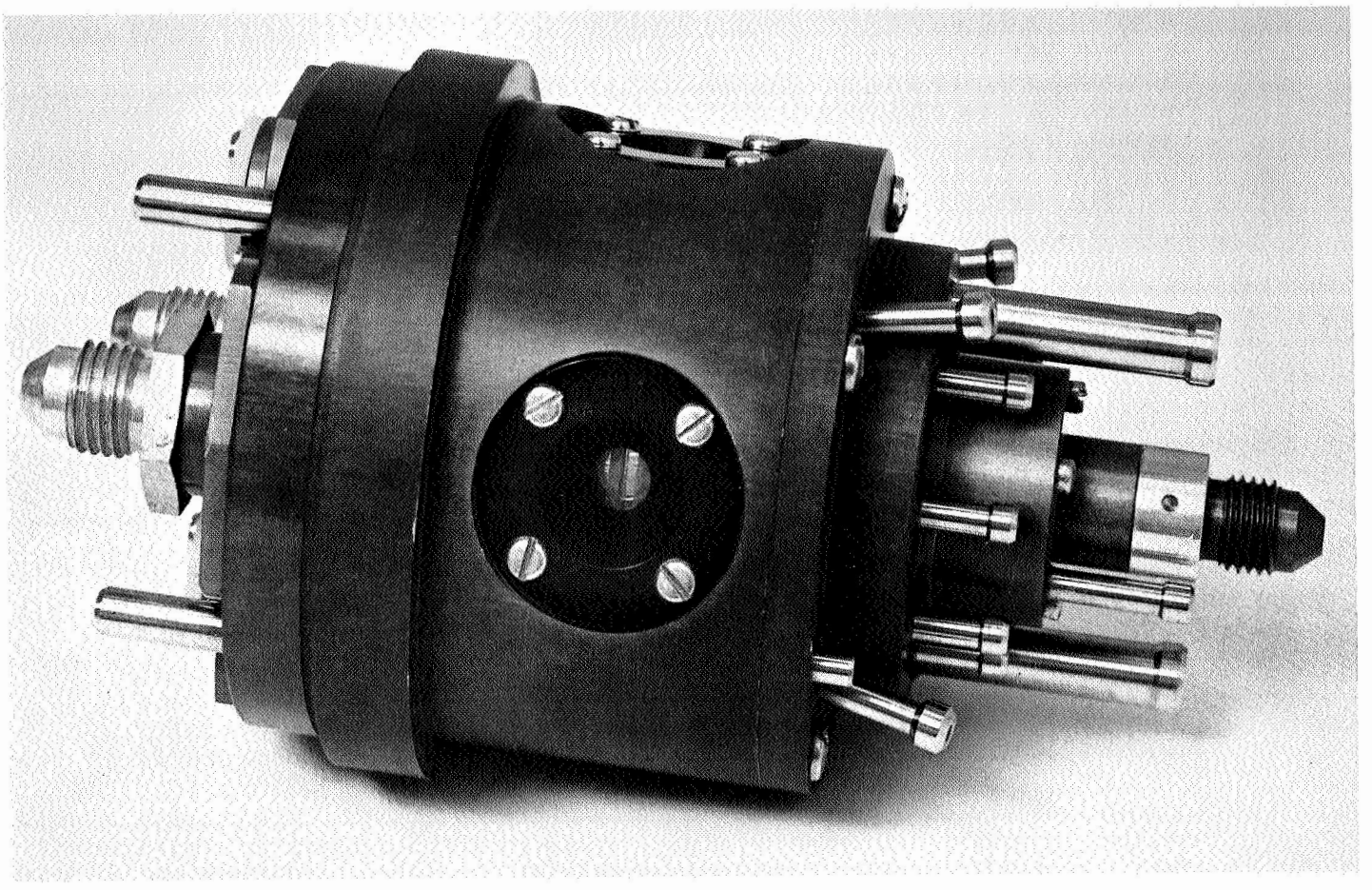

FIGURE 5 RGG-5A GYRO

The attitude of the rotor can be monitored by comparing the position of bands marked on the rotor, Figures 5 and 6, with a line scribed on the window at the nulled equator location. Since these bands extend somewhat less than 180 degrees around the rotor circumference, they can most readily be observed during high-speed operation by using a stroboscope, which also provides the means of rotor speed determination.

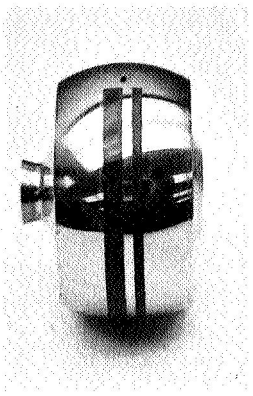

FIGURE 6 - RGG-5A GYRO ROTOR

TEST PROCEDURES AND RESULTS

Rotor-Stator Tests

Prior to the final assembly of the rotor-stator assembly, the bearing supply orifices in the stator assembly were subjected to several flow tests. Each individual restrictor was flow checked, and sets of restrictors matched within ±1 percent were selected for use in a given stator. After the restrictors were inserted in the stator, together with their filter discs, the individual flows were checked against each other again. The flows in the as-installed condition varied by as much as ± 20 percent. Repeated ultrasonic cleaning brought the divergence down to about ± 10 percent.

The rotors were then assembled on the stator assemblies, and each rotor was dynamically balanced on its own gas bearing to an estimated 20 micro ounce-inches. The axial static unbalance was next determined by orienting the rotor-stator assembly with its spin axis horizontal and observing the rate and direction of its precession in the horizontal plane by means of a laser-beam reflected off the flat side of the rotor. A stator-connected drift rate was observed to be present in both rotor-stator assemblies. This effect on the static balancing procedure was minimized by rotating the stator by trial and error until the stator-connected drift was predominantly in a vertical plane, and the static balance was then completed. It was qualitatively observed that the direction and rate of the stator-connected drift varied with the rotor angular attitude.

Gyro Test Setup

The gyro assemblies were set up and tested on a precision two-axis rotary table, Figure 7, which allows a full 360 degrees of rotational freedom about an axis which, in turn, can be rotated from vertical to horizontal about an east-west oriented trunnion. Individual pressure regulators controlled the pressures to the gyro bearing support, the rotor spin jets, the wide angle pickoff supply, the fine pickoff supply, each opposing pair of torquers, and each bias torquer. The wide angle pickoff differential output pressures were read on water-filled U-tube manometers, the fine pickoff differential output pressures on mercury-filled U-tube manometers, and the regulated supply pressures read on direct reading pressure gauges. Tygon supply and instrumentation flexible lines were employed to connect the gyro on the test table with the test bay.

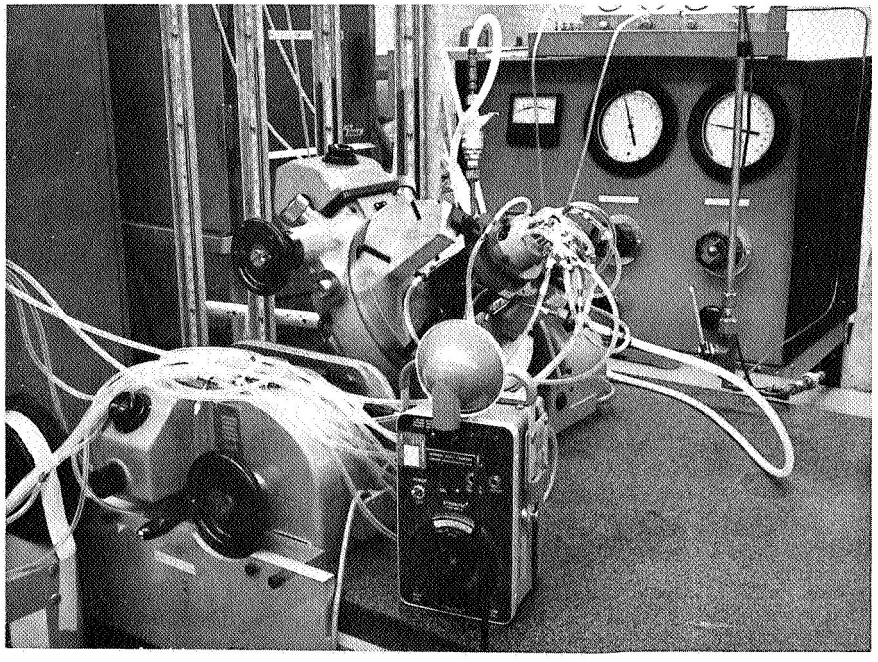

FIGURE 7 - TEST SETUP

Spin-up Tests

Several test runs were made to determine the start-up time required by the gyro. Since there is no mechanical caging means provided in the RGG-5A, the rotor was kept manually aligned during spin-up by the test operator, who monitored rotor angular position on the pneumatic pick-offs and applied the pneumatic torquers as required. Bearing pressure was applied to achieve rotor lift-off, followed by application of spin pressure. Rotor speed was determined by stroboscopic observation of the rotor markings through a case window. The time history of a typical start-up is presented in Figure 8.

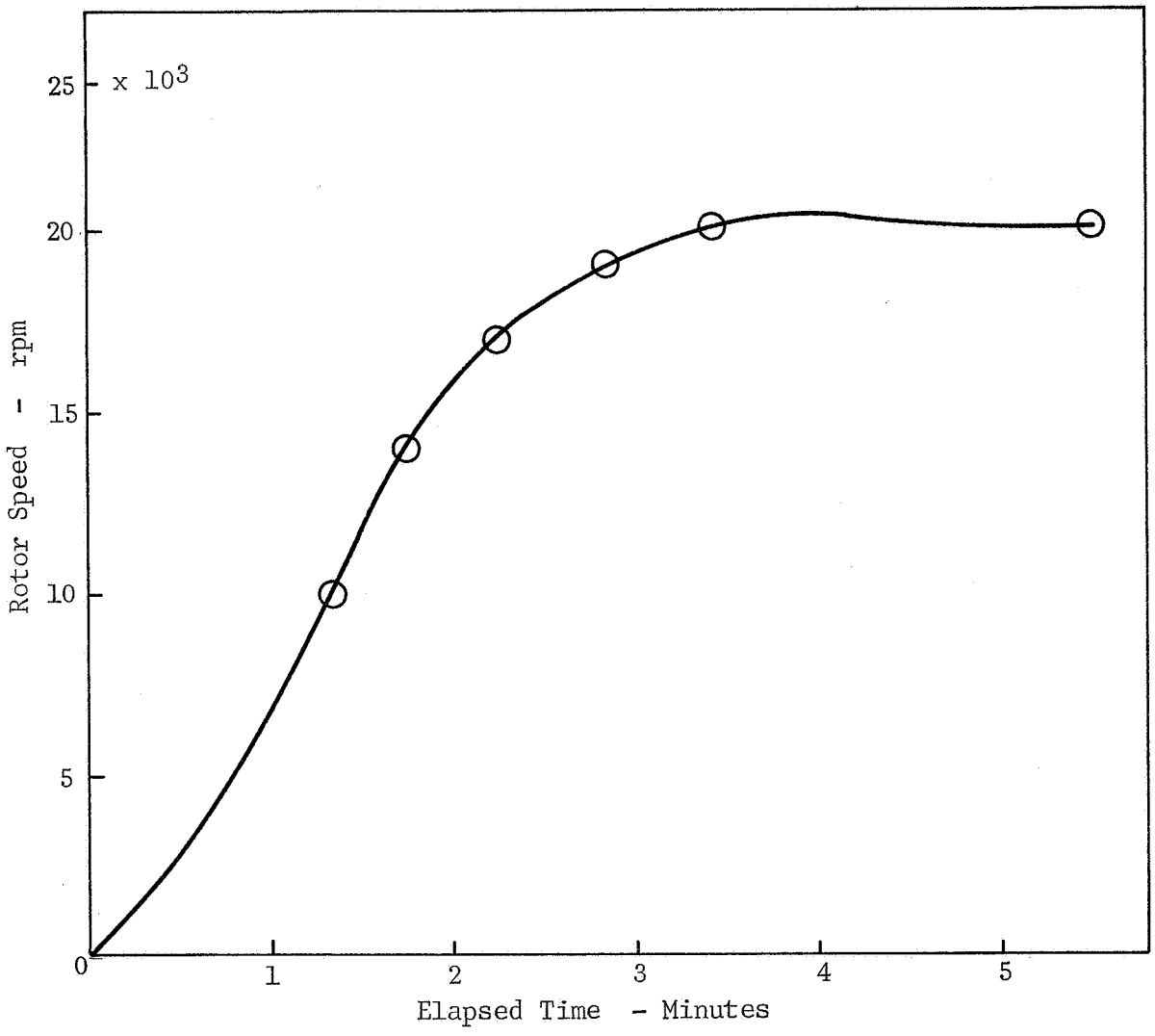

FIGURE 8 - START UP TIME HISTORY

Wide Angle Pickoff

The wide angle pickoff output pressure characteristics were determined over a range of ± 14 degrees of case-to-rotor relative angular deflection about each of the two sensitive axes. A pickoff supply pressure of 1 psig was used in all runs. The bias torquers were adjusted by trial and error to provide a minimum drift rate condition. The pickoff axes were squared-up with the table trunnion axis by rotating the table through small increments about the nominal zero setting and then elevating the table and gyro by means of the trunnion axis handwheel until a table setting was found at which only one pickoff output manometer responded to the movement. The pickoff calibration procedure consisted of precessing the rotor to its zero-zero position, as shown by the wide angle pickoff output manometers; tilting the case by elevating the table about the horizontal trunnion axis through the desired angle; reading the corresponding output pressure differential on its manometer; then returning the table to its initial setting and observing the residual manometer reading, if any, corresponding to the drift accumulated during the run. A range of ± 14 degrees by one-degree increments was covered using this procedure, and then the table was rotated 90 degrees about the table axis and the procedure was repeated to obtain the calibration about the second pickoff axis. The resulting pickoff calibrations are presented in Figure 9 for Serial No. 1, and Figure 10 for Serial No. 2. The input-output characteristics of the pickoffs are quite linear up to about ± 10 degrees, with the gain typically falling off at higher angular deflections. The pickoff gain averaged 1.05 in. H_2O (.038 psid)/degree for the Serial No. 1 gyro, and 1.28 in. H_2O (.046 psid)/degree for Serial No. 2. Pickoff coercive torques were not measured.

Fine Pickoff

The output characteristics of the fine pickoff in Serial No. 1 were also determined experimentally. A supply pressure of 20 inches of mercury was used; the resulting output pressure differential is shown in Figure 11, plotted against case-to-rotor deflection about each of the two sensitive axes. The nominal linear characteristics of the pickoffs are shown as dashed lines faired into the actual characteristics, shown solid. The fine pickoff in Serial No. 2 was inoperative and was not tested.

The linearized pickoff characteristics exhibit a gain of about 12 inches of mercury (5.9 psid)/degree over a region about 0.5 degrees wide and saturate beyond this region. The actual characteristics break sharply in the operating region, with two distinct slopes. The characteristic curves are biased away from symmetry about the zero pressure differential point, and they intersect at a point off the null defined by the wide angle pickoffs. The combination of nonlinear characteristics with the asymmetry of the characteristics about the zero point result in a zero point defined by these pickoffs which lies about 0.08 degrees away from the nominal and is in a region of lower gain (about 6 inches of mercury, or 2.9 psid/degree).

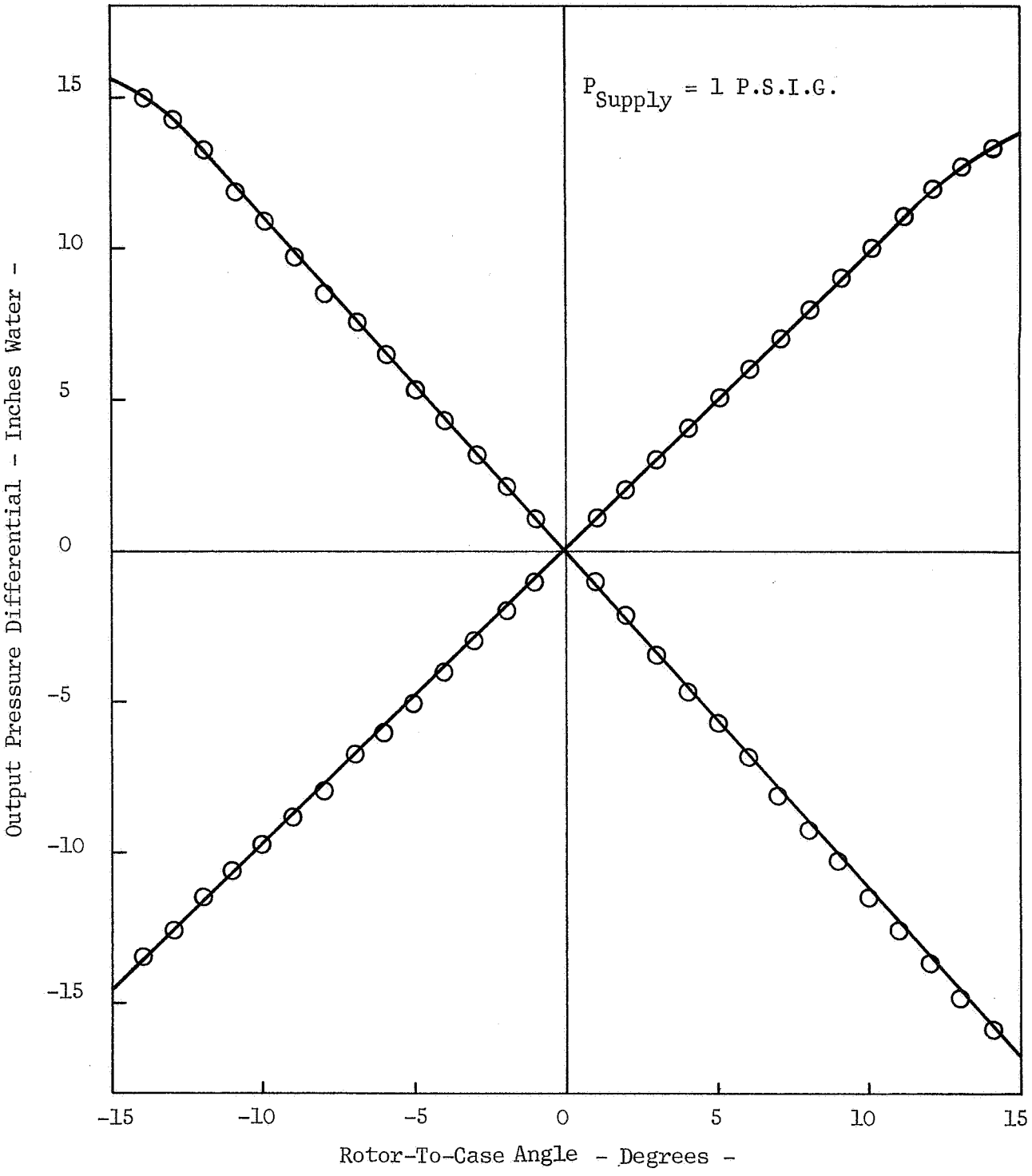

FIGURE 9 WIDE ANGLE PICKOFF CALIBRATION RGG-5A GYRO SERIAL #1

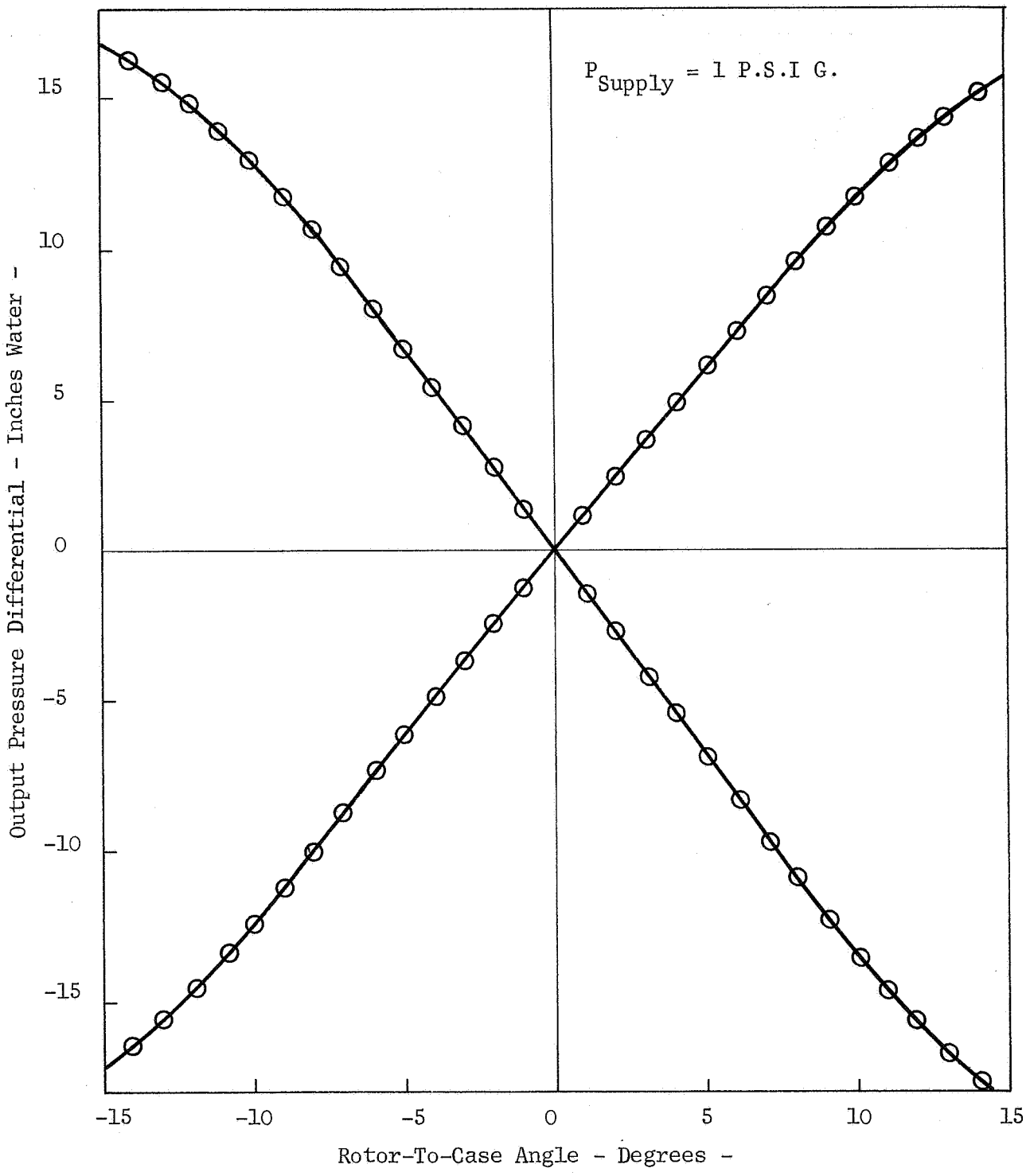

FIGURE 10 WIDE ANGLE PICKOFF CALIBRATION RGG-5A GYRO SERIAL #2

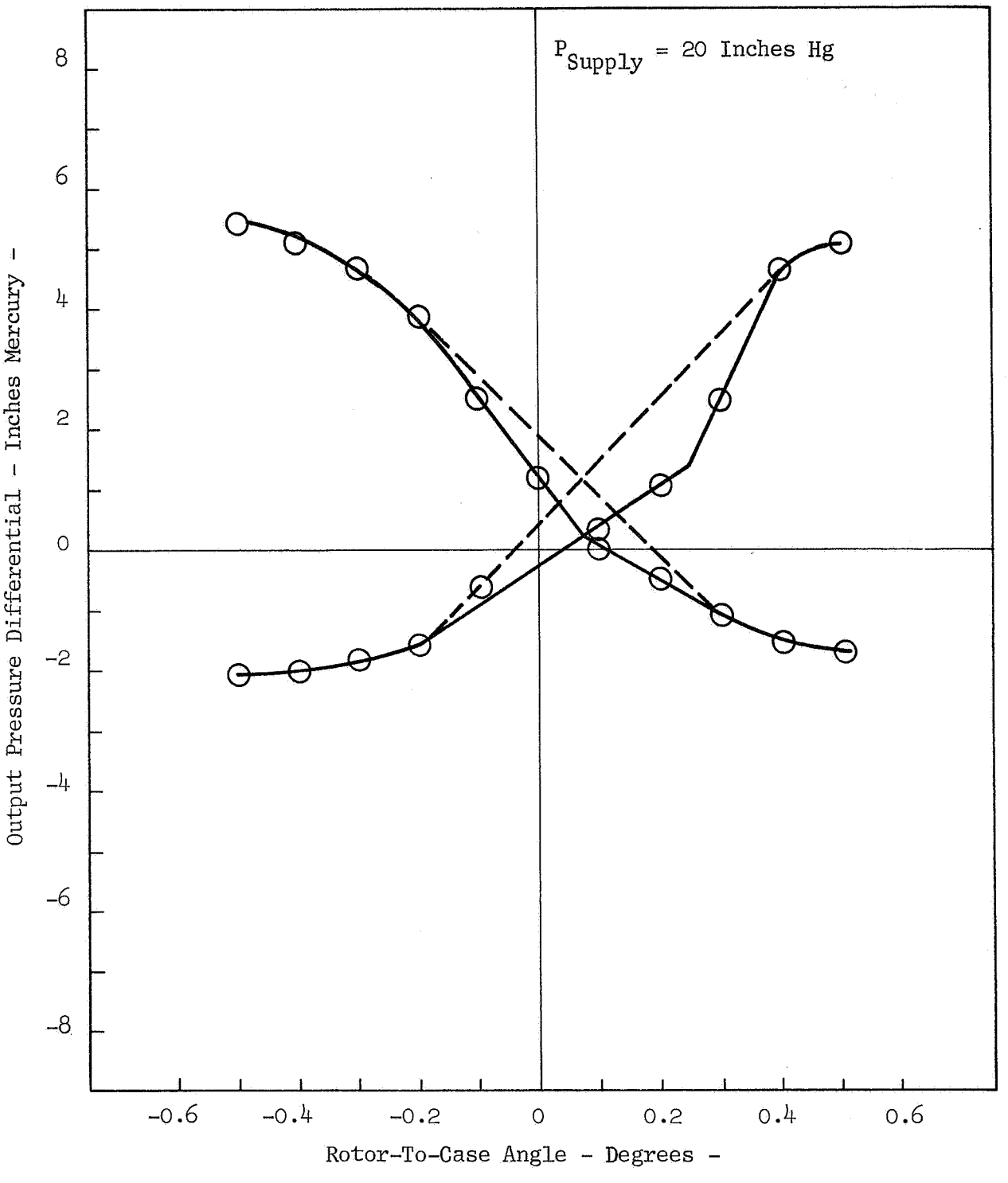

FIGURE 11 FINE PICKOFF CALIBRATION RGG-5A GYRO SERIAL #1

Torquers

Approximate calibrations of precession rate vs. input pressure were made on the gyro torquers, Figures 12 and 13. Due to limitations of the test setup, the input pressure was measured at the common supply to a toggle valve between two opposing torquers upstream of about 4 feet of 1/8 inch Tygon tubing, so the pressure drops due to these components are included in the input pressure values shown.

In the calibration procedure, the rotor was first precessed to zero the pickoff output manometers; then, with the torquer selector toggle valves closed, the torquer supply pressure was preset to the desired value. The proper toggle valve was then flipped open, activating the torquer, while simultaneously a stopwatch was started. As the torquer precessed the rotor, the table was tilted about its horizontal trunnion axis so as to keep the pickoff manometers at zero, thus providing a case rotation rate equal to the rotor precession rate. After a preselected time interval, the toggle valve was closed; and the increment in elevation angle about the trunnion axis was read on the table scale. A second toggle valve then was opened to the opposing torquer, and the procedure was repeated in the opposite direction of table elevation. Following the repetition of this procedure through a range of 2.5 to 30 psig by 2.5 psig increments, the table was rotated 90 degrees about the table axis; and the remaining two torquers were calibrated by the same method.

As shown in Figures 12 and 13, the precession rate varies approximately linearly with applied pressure, while comparison between these figures shows that the precession rate at a given applied pressure varies inversely with rotor speed. The mean torquer scale factor (disregarding Torquer No. 2 in Serial No. 1, which exhibits a scale factor 80 percent of the mean) can be determined from the test data by the following expression.

$$\text{Precession Rate}/_{\text{Pressure}} = \frac{K}{\text{Rotor Speed}} \tag{9}$$

$$K = \frac{\text{Rotor Speed (rpm)} \quad \text{Precession Rate (deg/min)}}{\text{Pressure (psig)}} \tag{10}$$

Substituting Serial No. 1 and Serial No. 2 data in this expression:

Serial No. 1 (Figure 12):

$$K = \frac{(1.34 \times 10^4)\ (32.5)}{(20)} = \underline{2.18 \times 10^4}\ \text{deg/min/psig/rpm}^{-1} \tag{11}$$

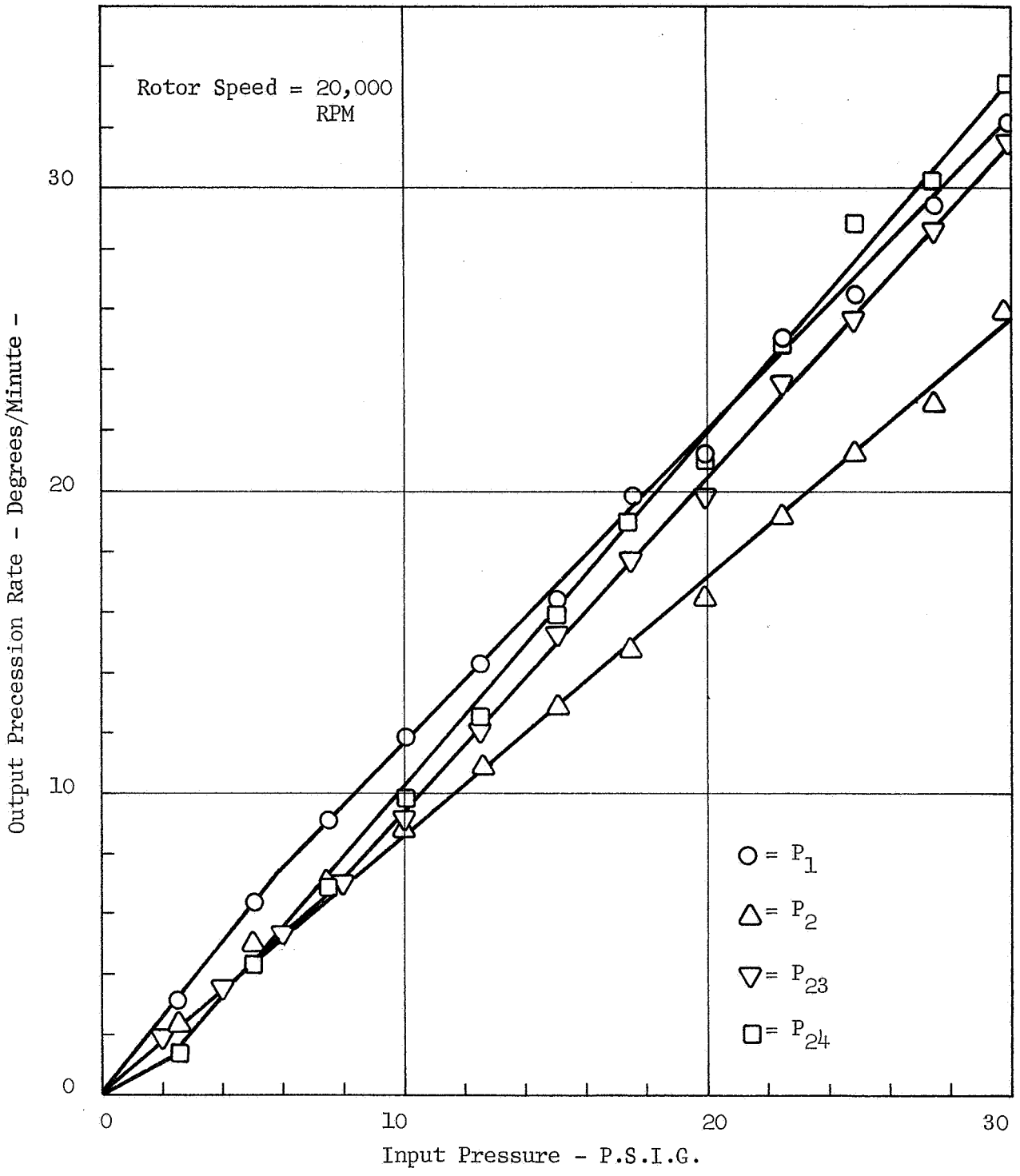

FIGURE 12 TORQUER CALIBRATION RGG - 5A GYRO SERIAL #1

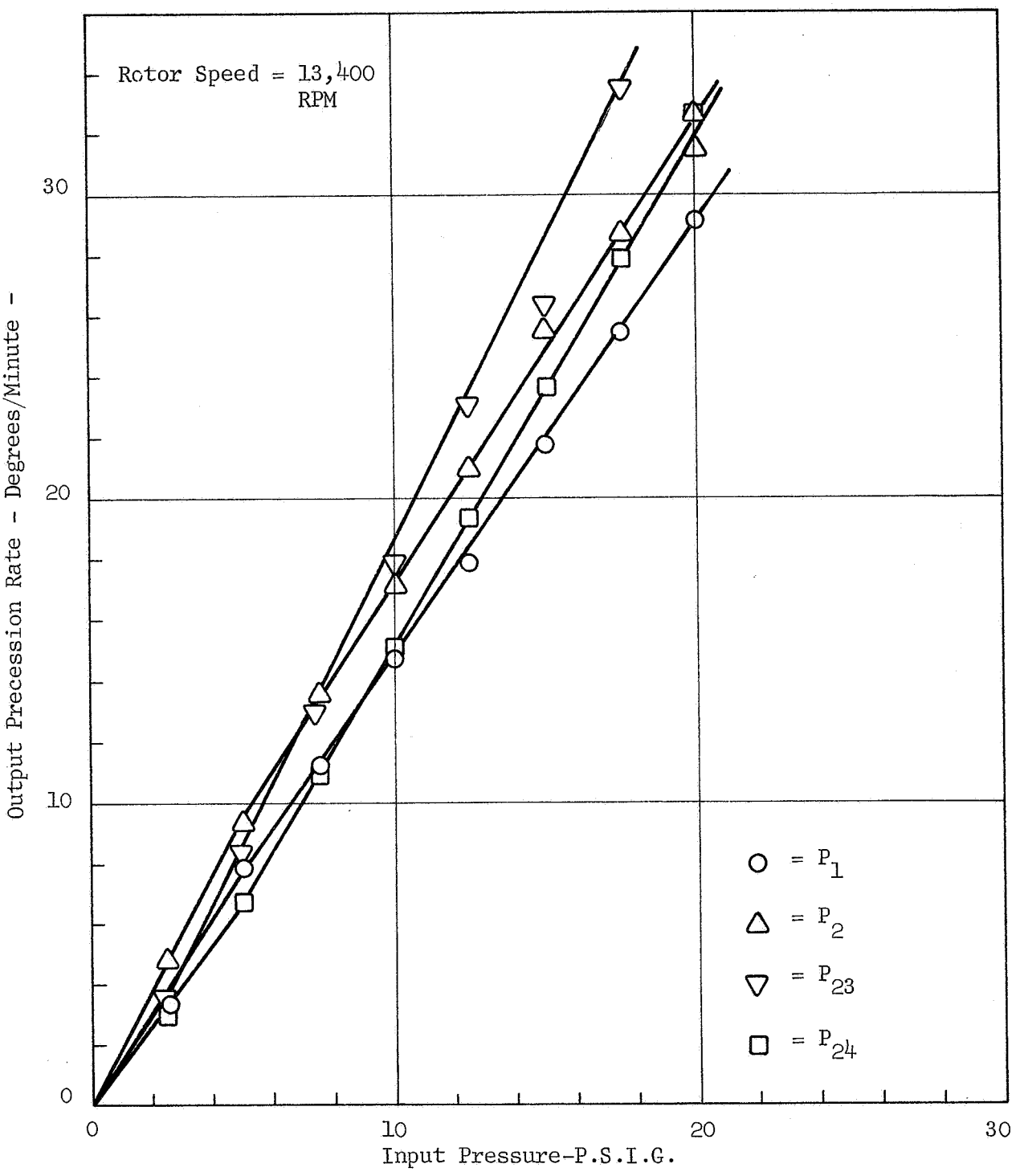

FIGURE 13 TORQUER CALIBRATION RGG-5A GYRO SERIAL #2

Serial No. 2 (Figure 13):

$$K = \frac{(2.0 \times 10^4)\ (32.6)}{(30)} = \underline{2.17 \times 10^4}\ \text{deg/min/psig/rpm}^{-1} \qquad (12)$$

It is apparent that the mean torquer scale factor is the same for the two gyros, indicating that the torque exerted is independent of speed.

An additional series of runs, not shown, was made in which the torquer was applied for a preset time (.5 to 1 minute) with the table fixed so that the rotor was precessed from its null position, and the change in rotor attitude read from the wide angle pickoff manometers. The results agreed with those obtained by the method described above, indicating that the mean torquer scale factor is independent of rotor-to-case angle as well.

The bias torquers were employed in the drift testing, but they were not separately calibrated.

Drift Tests

A large number of drift runs were made on the two units, with and without bias torquer compensation, and with horizontal, vertical, and polar orientations of the spin axis. Drift runs were made by initially precessing the rotor to zero the wide angle pickoff output manometers, starting a stopwatch, and reading the wide angle pickoff output manometers at the end of each test time interval (typically one-minute intervals were used). The drift data discussed below was taken with the gyro spin axis initially aligned parallel to the spin axis of the earth, in order to eliminate the systematic contribution of earth rate.

Since this is a two-axis gyro, the means of plotting the time history of the drift runs and determining the resulting drift rate is subject to some interpretation. Typically, the drift rate about one axis was less than that about the other, so that the most favorable interpretation would be to select the data from the low drift rate axis. In an application, however, the total drift rate from the initial heading is the significant quantity in evaluation of system performance. The drift rate presented below, therefore, is the total drift rate; i.e., the resultant or square root of the sum of the squares of the drift rate about each axis. Therefore, these values are at each point at least equal to the maximum rate about the worst drift axis.

It was found that when properly biased, both units exhibited low drift rates when the rotor was aligned with the stator; but the drift rate increased with larger rotor-to-stator angles. These trends are clearly shown by Figures 14 and 15 for the Serial No. 1 gyro, and Figure 17 for the Serial No. 2 gyro. These figures show that bias torquers can be adjusted to maintain the mean drift rate less than 1 degree/hour for periods of 10 to 30 minutes, but that eventually the rotor angular displacement exceeds some threshold value and the drift rate then grows more rapidly. Figure 16 shows the time history of one run on Serial No. 1 gyro, in which the displacement never crossed this threshold and the spin axis drifted randomly near the origin for a two-hour period with a maximum

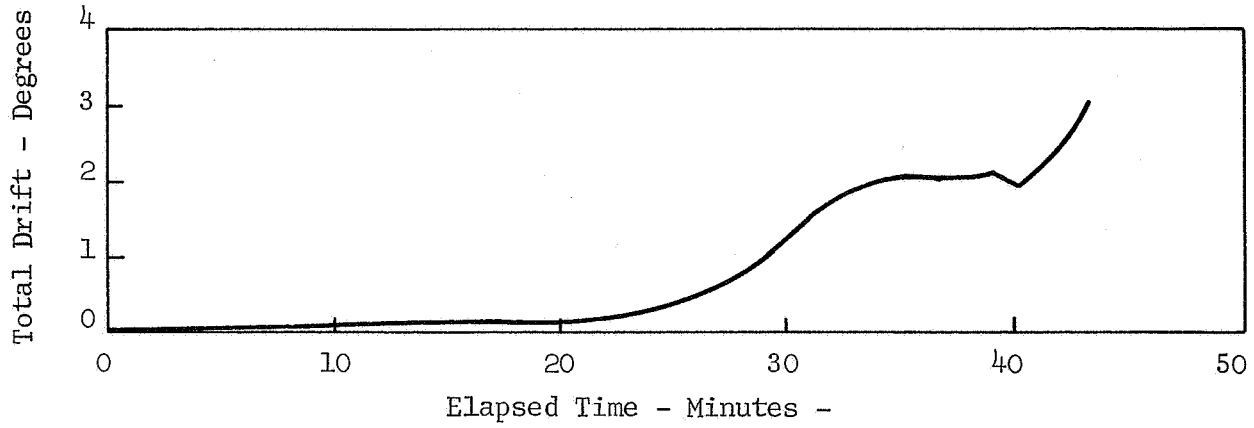

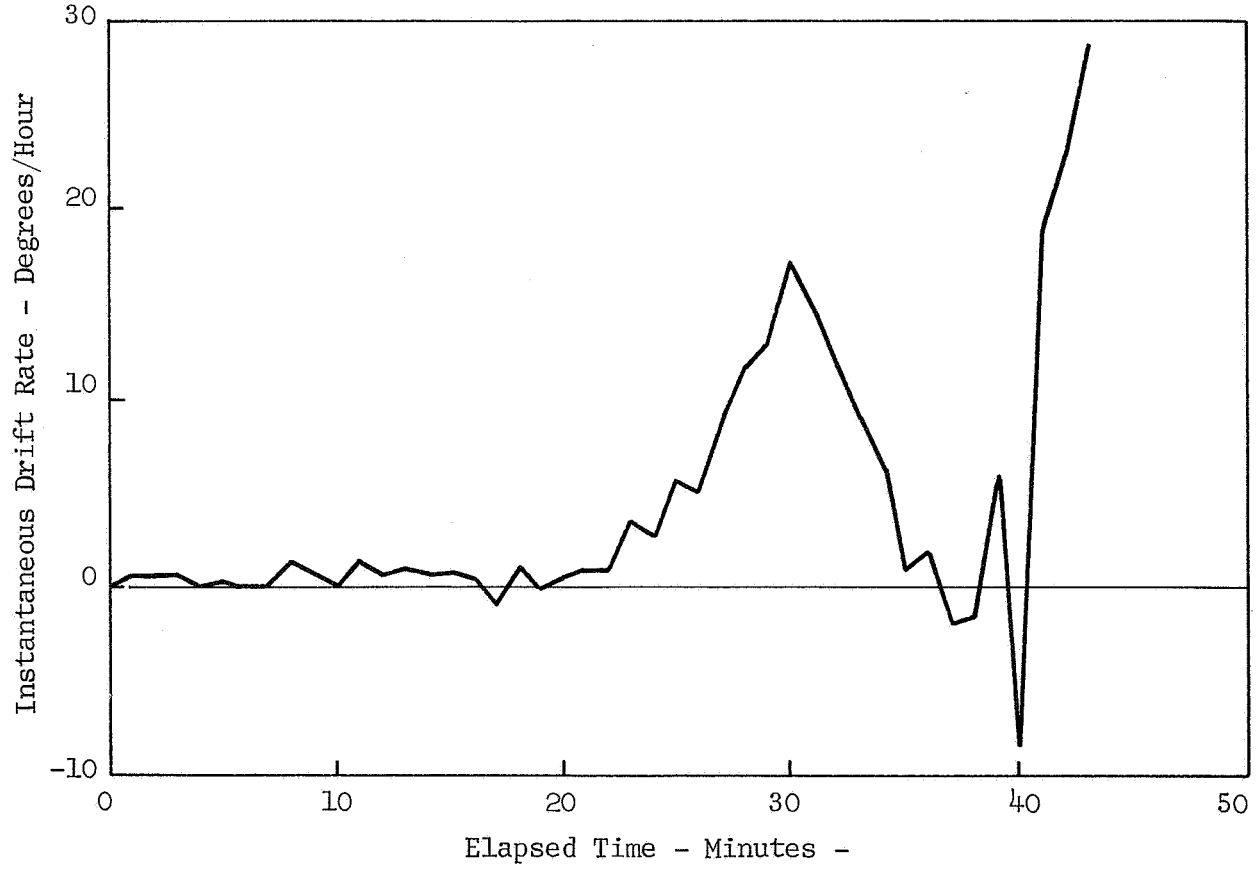

FIGURE 14 DRIFT TEST RUN #9 - 6 JUNE RGG-5A GYRO SERIAL #1

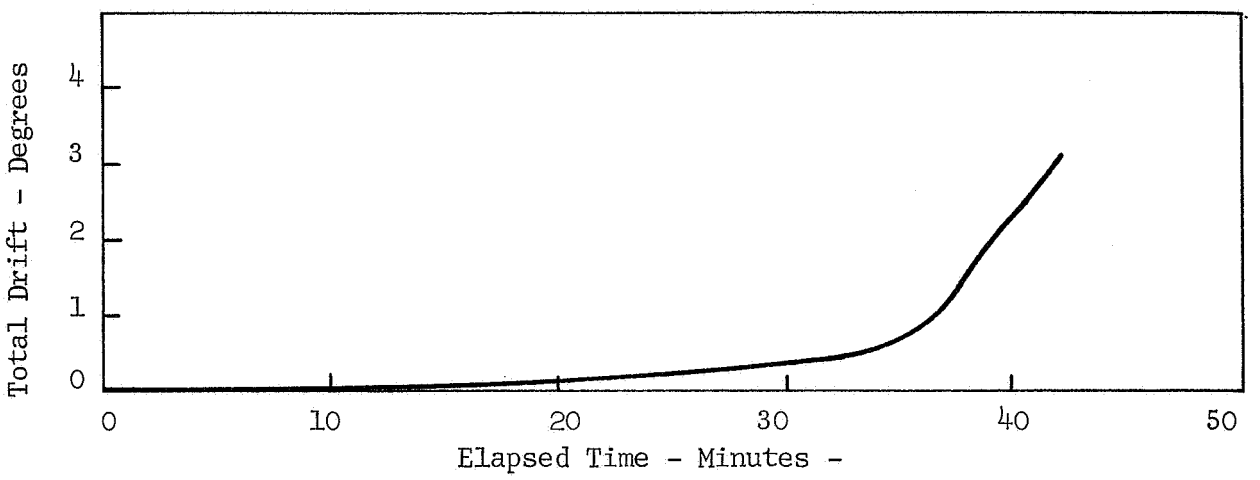

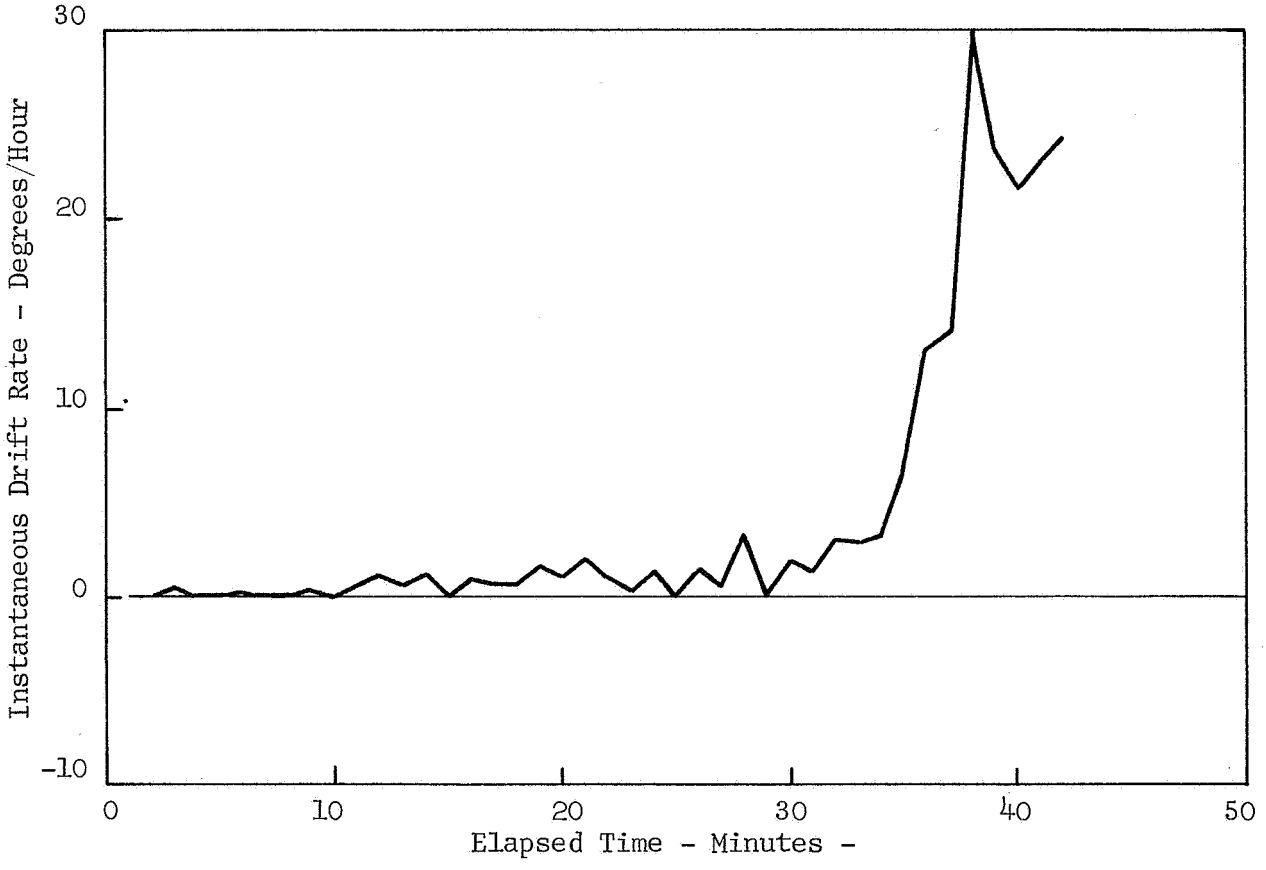

FIGURE 15 DRIFT TEST RUN #11 - 6 JUNE RGG-5A GYRO SERIAL #1

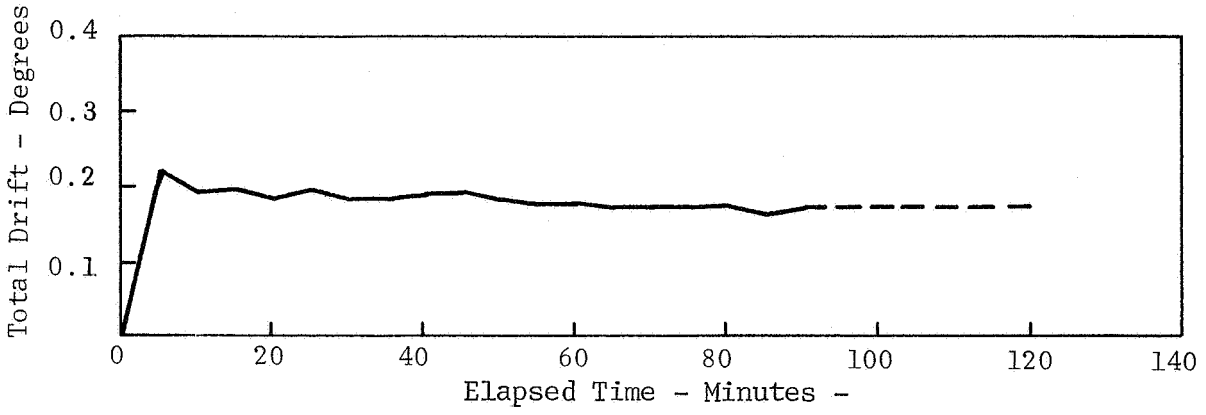

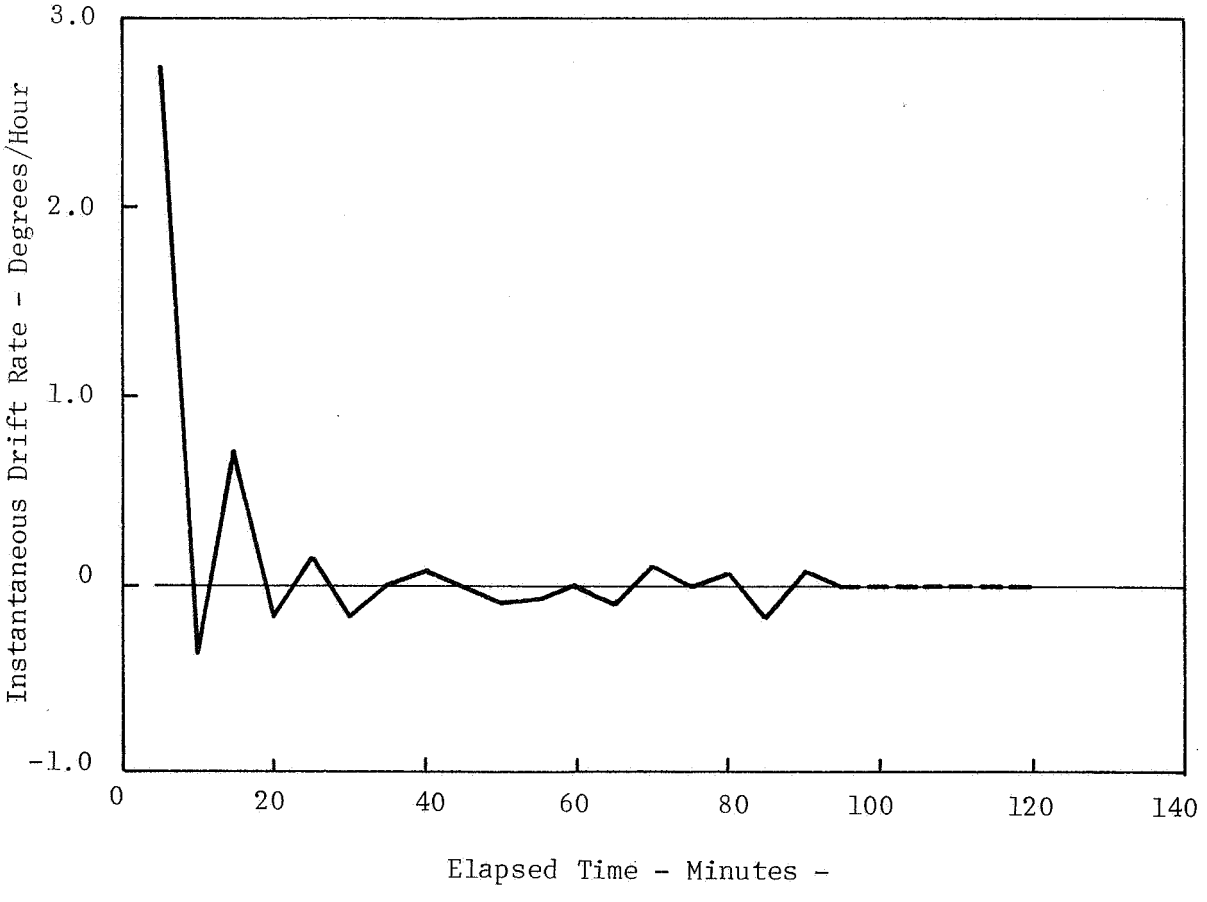

FIGURE 16 DRIFT TEST RUN #3 - 7 JUNE RGG-5A GYRO SERIAL #1

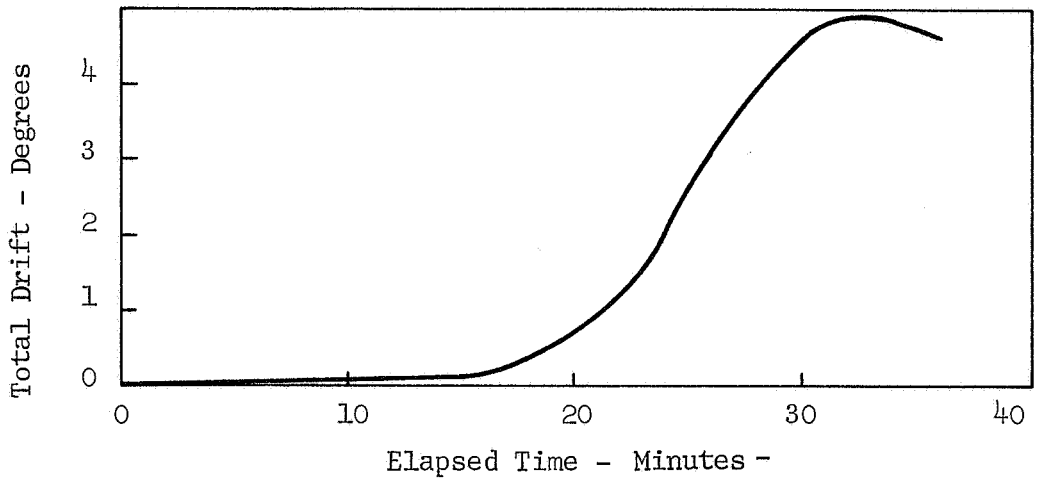

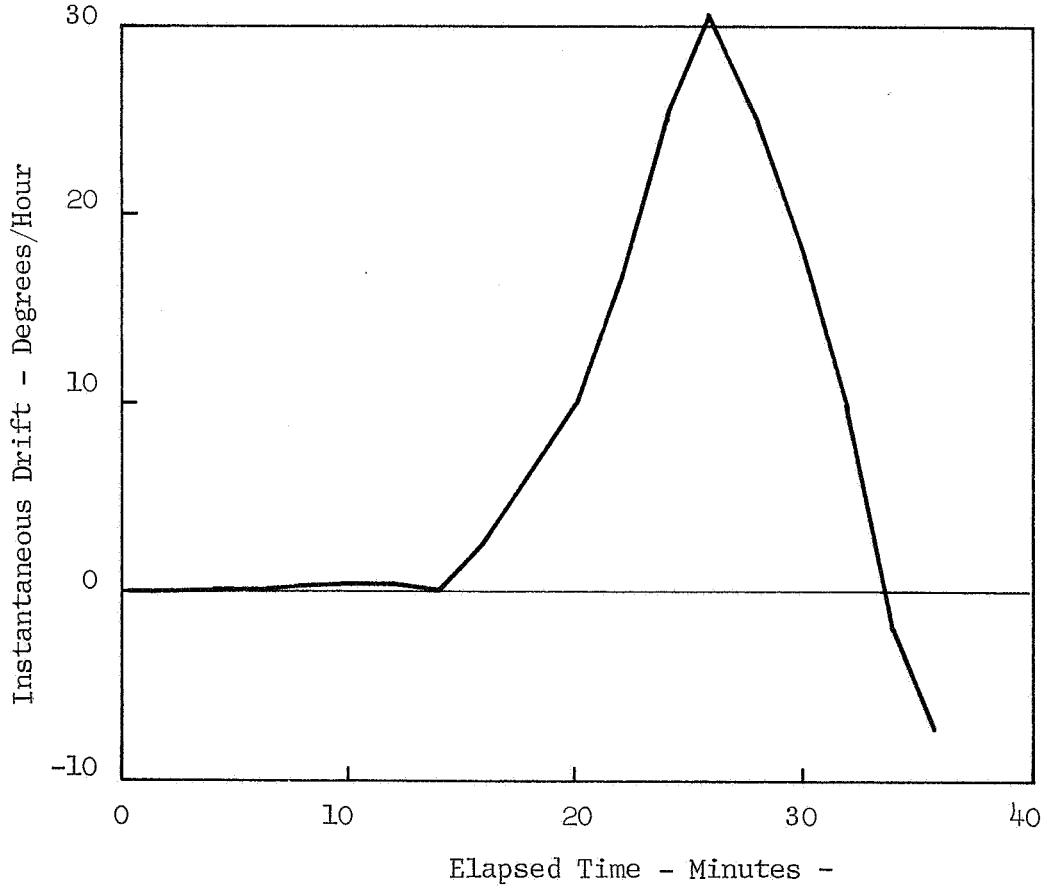

FIGURE 17 DRIFT TEST RUN #7 - 21 JUNE RGG-5A GYRO SERIAL #2

drift rate (taken over five-minute reading intervals) of .36 degree/hour following an initial transient. The sample standard deviation, S, of the random drift on this run was .134 degree/hour after 90 minutes. The major characteristics of these runs are presented below in Table 2.

TABLE 2

Summary of Drift Performance

Serial No. 1: Run 9 (6 June 1968)

in first 22 minutes

Sample standard deviation = .7920 degree/hour (maximum)
Maximum inst. rate = 1.32 degree/hour
Total drift in 22 minutes = .201 degree
Mean drift rate = $.201 \times \frac{60}{22} = .55$ degree/hour

Serial No. 1: Run 11 (6 June 1968)

in first 27 minutes

Sample standard deviation = .9064 degree/hour (maximum)
Maximum inst. rate = 2.04 degree/hour
Total drift in 27 minutes = .294 degree
Mean drift rate = $.294 \times \frac{60}{27} = .65$ degree/hour

Serial No. 1: Run 3 (7 June 1968)

over 2-hour period

Sample standard deviation = .367 degree/hour (about value after first 5 minutes, maximum).
Maximum inst. rate = 2.68 degree/hour (.36 degree/hour if eliminate first 5 minutes).
Total drift in 2 hours = .172 degree (.051 degree from offset after 5 minutes).
Mean drift rate = .086 degree/hour (.026 degree/hour from offset after 5 minutes).

Serial No. 2: Run 7 (21 May 1968)

in first 14 minutes

Sample standard deviation = .442 degree/hour (maximum)
Maximum inst. rate = .633 degree/hour
Total drift in 14 minutes = .080 degree
Mean drift rate = $.080 \times \frac{60}{14} = .34$ degree/hour

DISCUSSION OF TEST RESULTS

The purpose of the test phase of this program was to determine the functional characteristics of the gyroscope and to evaluate the actual performance vis-a-vis the goals listed in the work statement. The functional characteristics are described by the test results of the preceding section. This section presents an item-by-item comparison between the work statement goals and the gyro performance as shown by test results. Each of the performance goals is listed below, followed by a discussion of the corresponding test data.

"0.5 to 1 Degree/Hour Drift"

The data shown in Figures 14 through 17, and Table 2, demonstrates the ability of the RGG-5A Gyro to maintain its initial heading with a mean drift rate of .35 to .65 degree/hour over a 14 to 27 minute period. Consideration should be given to the increase in drift rate (to as much as 1 degree/minute) with increasing rotor-to-case angular deviation. The implication of this performance characteristic is that vehicle pointing accuracy in the 0.1 to 1.0 degree/hour drift range can be achieved with the present performance of the RGG-5A Gyro if the rotor-to-case angular deflection remains small. Although this performance does not satisfy space probe requirements in which wide angle, low drift performance is important, it should prove adequate for other applications.

"Plus or Minus 15 Degree Operating Angular Freedom"

The layout of the gyro provides a total angular freedom of ± 17 degrees. The pickoff calibrations, Figures 9 and 10, demonstrated their operation to ± 14 degrees about both input-output axes. An examination of the drift data (Figures 14, 15, and 17), however, shows that the operational utilization of the ± 15 degree angular freedom provided imposes a significant penalty in drift rate on the gyro.

The stator-centered drift exhibited by the rotor-stator assembly outside the case, as described earlier, is thought to be a major contribution to this off-axis increase in drift rate. Qualitative tests on the rotor-stator assembly in the course of static-balancing the rotor showed the magnitude of the stator-centered drift to be unaffected by rotor speed, but evinced a sensitivity to rotor angle in both magnitude and direction of drift. The former observation indicates that the drift inducing torque increases proportionately with speed, suggesting a viscous shear mechanism such as the so-called turbine torques induced by flow unbalances or geometric imperfections in the gas bearing. Although the jewel primary restrictions in the gas bearing were matched on the basis of flow checks prior to assembly in the stator, post assembly flow checks showed about a ± 10 percent variation in flow from restrictor to

to restrictor in the stator. In addition, there was some evidence that processing to which the rotors were subjected during nickel-plating preparation by an outside vendor removed material unevenly from the bearing surface of the rotor, altering its as-lapped dimensional geometry.

Due to program time limitations, these deviations from ideal were accepted but were probably the cause of at least a significant portion of the observed off-axis drift. The author plans further investigation of the causes of and remedies for the off-axis drift following the conclusion of this program.

"Erection Alignment Capability of 2 to 3 Arc-Minutes"

The RGG-5 Gyro has no mechanical caging mechanism. Initial erection of the rotor is intended to be accomplished by means of a high-gain external fluidic control loop which, when activated, amplifies the error signals from the pickoffs and applies corresponding pressure signals to the torquers, precessing the rotor to the erected position. The erection alignment capability by this means depends on the threshold and gain of the fluidic amplifier, the gain and signal/noise resolution of the pickoff, and the disturbance torque level of the rotor as measured by the torquer pressure required to overcome the velocity induced by the disturbance. A prominent manufacturer of flueric operational amplifiers quotes values of gain = 2000 and threshold = 10^{-4} to 10^{-5} psid, for his product. The test data shows gains of about .040 psid/degree or 6.7×10^{-4} psid/arc-minute for the wide angle pickoffs, and 2.9 psid/degree or 4.8×10^{-2} psid/arc-minute for the fine pickoffs. The resolution of the wide angle pickoffs was found to be at least equal to the smallest reading on the instrumentation used, .01 inch of water or 4×10^{-4} psid. The resolution of the fine pickoff was not determined. The torquer gains at 20,000 rpm were approximately 1 degree/minute per psig or 60 degrees/hour per psig, while the disturbance drift rate to be overcome was 1 degree/hour or less in the vicinity of the erection position.

The erection alignment capability of a proportional control loop with the above component gains and thresholds can now be evaluated. The torquer input required to offset the drift torque at null is approximately 1.7×10^{-2} psig $\left(1 \text{ deg/hr} \Big/ \frac{60 \text{ deg/hr}}{\text{psig}}\right)$. The amplifier gain required to provide this torquer pressure, with a position error of 1 arc-minute providing a wide angle pickoff output pressure signal of 6.7×10^{-4} psid, is $25 \left(1.7 \times 10^{-2} \text{ psig} \Big/ 6.7 \times 10^{-4} \text{ psid}\right)$. This value of amplifier gain is far lower than that achievable by the operational amplifier, while the assumed pickoff pressure signal is larger than the threshold values of both the pickoff and the amplifier. Consequently, an erection alignment capability of less than 2-3 arc-minutes has been demonstrated. Note that use of the fine pickoff could provide improved accuracy of alignment, if desired.

"Spin-up and Alignment Time
of 5 to 10 Minutes"

The time history of gyro start-up given in Figure 8 shows that spin-up to terminal speed of just over 20,000 rpm and manual alignment took place in 5-1/2 minutes. Other runs have shown that even shorter spin-up times can be obtained by exceeding the steady-state spin pressure until terminal speed is reached, and then cutting spin pressure back. This performance goal was met.

"Maximum Precession Capability of Torquer,
30 Degrees/Minute"

As shown in Figures 12 and 13, the torquers exhibited a linear precession rate vs. pressure characteristic with a maximum value of precession rate of 32.5 degrees/minute demonstrated. This performance goal was met.

CONCLUSIONS

The design and construction of a wide angle, all-pneumatic, free gyroscope was successfully carried out; and its novel features, as well as its performance as an inertial instrument were experimentally demonstrated. The two-axis, wide angle fluidic pickoff exhibited a linear characteristic with a gain of .038 to .046 psig/degree at a supply pressure of 1 psg out to ± 10 degrees and excellent resolution out to ± 14 degrees (the limit of testing) with a reduced gain. The torquers also exhibited linear behavior with a scale factor of 2.18×10^4 degrees/minute/psig/rpm^{-1}, and a precession capability of 30 degrees/minute. The wide angle rotor support gas bearing demonstrated its ability to allow rotor angular travel of ± 14 degrees about both axes, with an untested design margin of 3 degrees provided above this value. Mean gyro drift rates between .35 and .65 degrees/hour were demonstrated for small rotor angular deviations from null, although the drift rate increased materially at larger rotor angular deviations.

RECOMMENDATIONS FOR FURTHER WORK

The construction of the RGG-5A all-pneumatic, free gyroscope is a significant milestone on the road to the utilization of fluidic inertial systems in operational vehicles. Depending on the potential application considered, however, a number of tasks remain to be accomplished. These tasks fall into two categories: improvement of specific aspects of gyro design, and resolution or solution of application factors. Several examples of each are listed as follows.

1. Provision of fluidic speed control or compensation means on the gyro to allow precise torque-precession rate relation to be held.

2. Design and implementation of external fluidic closed-loop system to provide initial erection means and to allow closed-loop testing and operating modes.

3. Modification of RGG-5A circuitry to allow operation on single regulated pressure input as opposed to individual pressure regulators presently required.

4. Continued effort to improve drift performance, particularly in the area of large rotor angular deviations from null.

5. Perform standard performance tests for inertial grade gyros on modified units.

6. Study of the interfacing between the fluidic gyro and the remainder of the vehicle flight control system.

Western Development Center,
Conductron Corporation,
Northridge, California - July 8, 1968

REFERENCES

1. Henley, W. H.; and Christopher, Philip A.: "Feasibility Study of An All-Pneumatic Wide Angle Free Gyroscope." NASA CR-66334, 1967.

NASA CR-66675

DISTRIBUTION LIST

NAS1-7570

	Copies
NASA Langley Research Center Langley Station Hampton, Virginia 23365	
Attention: Research Reports Division, Mail Stop 122	1
R. L. Zavasky, Mail Stop 117	1
Technology Utilization Office, Mail Stop 103	1
H. Douglas Garner, Mail Stop 494	12
Richard F. Hellbaum, Mail Stop 494	1
NASA Ames Research Center Moffett Field, California 94035	
Attention: Library, Stop 202-3	1
Curtis L. Muehl, Mail Stop 213-2	1
NASA Flight Research Center P. O. Box 273 Edwards, California 93523	
Attention: Library	1
Rodney K. Bogue	1
Jet Propulsion Laboratory 4800 Oak Grove Drive Pasadena, California 91103	
Attention: Library, Mail 111-113	1
NASA Manned Spacecraft Center 2101 Webster Seabrook Road Houston, Texas 77058	
Attention: Library, Code BM6	1
NASA Marshall Space Flight Center Huntsville, Alabama 35812	
Attention: Library	1
NASA Wallops Station Wallops Island, Virginia 23337	
Attention: Library	1
NASA Electronics Research Center 575 Technology Square Cambridge, Massachusetts 02139	
Attention: Library	1
Edwin H. Hilborn, Code GCD	1
NASA Lewis Research Center 21000 Brookpark Road Cleveland, Ohio 44135	
Attention: Library, Mail Stop 60-3	1
Vernon D. Gebben, Mail Stop 86-6	1
William S. Griffin, Mail Stop 86-6	1
Lyle O. Wright, Mail Stop 54-4	1

NASA CR-66675

DISTRIBUTION LIST

NAS1-7570

	Copies
NASA Goddard Space Flight Center Greenbelt, Maryland 20771 Attention: Library	1
NASA John F. Kennedy Space Center Kennedy Space Center, Florida 32899 Attention: Library, Code IS-CAS-42B	1
National Aeronautics and Space Administration Washington, D. C. 20546	
Attention: Library, Code USS-10	1
Carl Janow, Code REC	1
NASA Code RE	1
U. S. ATAC, AMSTA-Z Warren, Michigan 48090 Attention: Gregory Arutunian	1
Naval Air Propulsion Test Center Aeronautical Engine Department Philadelphia, Pennsylvania 19112 Attention: Joseph A. Avbel	1
Watervliet Arsenal Watervliet, New York 12189 Attention: John A. Barrett	1
Frankford Arsenal Philadelphia, Pennsylvania 19137	
Attention: Wilbert F. Buie, SMUFA-J52/00-220-1	1
Robert A. Shaffer, SMUFA-M-2200	1
Manuel Weinstock, SMUFA-J5400-220-1	1
Commanding Officer U. S. Army Combat Developments Commany Air Defense Agency Fort Bliss, Texas 79916 Attention: Captain Chen, GSGAD-M	1
Picatinny Arsenal Dover, New Jersey 07801	
Attention: Anthony P. Corrado, SMUPA-TT-2	1
George R. Taylor, NED AADL-B65	1
Naval Ship Systems Command Ships 03414 Washington, D. C. 20360 Attention: Art Chaikin	1
Department of the Navy Washington, D. C. 20360	
Attention: Ancel E. Cook, ONR, Code 403C	1
David S. Siegel, ONR, Code 461	1

NASA CR-66675

DISTRIBUTION LIST

NAS1-7570

	Copies
U. S. Naval Avionics Facility 6100 E. 21 Street Indianapolis, Indiana 46218 Attention: Robert K. David, D/830	1
U. S. Army Corps of Engineers Huntsville Division P.O. Box 1600, West Station Huntsville, Alabama 35807 Attention: M. Dembo, HNDSE-R	1
Harry Diamond Laboratories Washington, D. C. 20438 Attention: Evan D. Fisher, Br. 430 Richard N. Gottron, Br. 310 Joseph M. Kirshner, Br. 310 Kenneth R. Scudder, Br. 310 Raymond W. Warren, Br. 430	1 1 1 1 1
USAAVLABS Fort Eustis, Virginia 23604 Attention: George W. Fosdick	1
Pacific Missile Range Point Mugu, California 93041 Attention: Abram J. Garrett, Technical Support Dept., Box 10	1
Naval Weapons Center Weapons Development Department China Lake, California 93555 Attention: Rolf O. Gilbertson, Code 4044	1
Army Missile Command Redstone Arsenal, Alabama 35809 Attention: William A. Griffith, AMSMI-RGC Thomas G. Wetheral, AMSMI-RGC, Bldg. 5400	1 1
AFFDL (FDCL) Wright-Patterson Air Force Base, Ohio 45433 Attention: James F. Hall	1
Naval Weapons Center Corona Laboratory Corona, California 91270 Attention: Stanley F. Johnson, Code 75	1
Headquarters, U. S. Army Materiel Command Washington, D. C. 20315 Attention: Daniel J. Jones, AMCRD-RP	1

NASA-CR-66675

DISTRIBUTION LIST

NAS1-7570

	Copies
NAVSEC Philadelphia Division Philadelphia, Pennsylvania 19112 Attention: Irvin N. Kenig, Code 6772	1
Naval Air Systems Command 18th and Constitution Avenues, N. W. Washington, D. C. 20360 Attention: Richard A. Retta, AIR-52022	1
AFRPL (RPREA) Edwards, California 93523 Attention: K. O. Rimer	1
AFOSR 1400 Wilson Boulevard Arlington, Virginia 22209 Attention: Milton Rogers	1
NAVSEC Main Navy Building Washington, D. C. 20360 Attention: Wilbert L. Smith, Code 6147E	1
Headquarters, SAAMA, SANEPA Kelly Air Force Base, Texas 78241 Attention: Capt. Fred Kopper	1
U. S. Atomic Energy Commission Division of Reactor Development Washington, D. C. 20545 Attention: Frank C. Legler	1
Department of the Army Office of Chief of Research & Development Washington, D. C. 20310 Attention: Major B. P. Manderville, Jr., CRDPES	1
Naval Applied Science Laboratories Flushing and Washington Avenues Brooklyn, New York 11251 Attention: Philip Marino, Code 926	1
Naval Missile Center Point Mugu, California 93041 Attention: Stanley N. Opatowsky, Code 5351, Box 15	1
Naval Air Engineering Center Philadelphia, Pennsylvania 19112 Attention: Harold N. Ott (WESOX-24)	1

NASA CR-66675

DISTRIBUTION LIST

NAS1-7570

	Copies
U. S. Naval Ordnance Laboratory White Oak, Silver Spring, Maryland 20910 Attention: Charles F. Peer	1
U. S. Electronics Proving Ground Fort Huachuca, Arizona 85613 Attention: Lt. William Peterson, STEEP-DC-C	1
Air Force Avionics Laboratory Wright-Patterson Air Force Base, OHio 45433 Attention: Major Roi F. Prueher, Plans Office	1
Naval Air Development Center Johnsville, Pennsylvania 18974 Attention: Horace Welk	1
Headquarters, U. S. Air Force Washington, D. C. 20301 Attention: Lt. Comdr. Carl Wheaton (AFRDDE)	1
AFWL Kirtland Air Force Base, New Mexico 97117 Attention: Lt. John J. Wozniak	1
NASA Scientific and Technical Information Facility P. O. Box 33 College Park, Maryland 20740	21 plus reproducible